Dynamics of comb-of-comb-network polymers in random layered flows

Divya Katyal and Rama Kant*
Complex Systems Group, Department of Chemistry, University of Delhi, Delhi 110007, India
(Received 26 September 2016; published 27 December 2016)

We analyze the dynamics of comb-of-comb-network polymers in the presence of external random flows. The dynamics of such structures is evaluated through relevant physical quantities, viz., average square displacement (ASD) and the velocity autocorrelation function (VACF). We focus on comparing the dynamics of the comb-of-comb network with the linear polymer. The present work displays an anomalous diffusive behavior of this flexible network in the random layered flows. The effect of the polymer topology on the dynamics is analyzed by varying the number of generations and branch lengths in these networks. In addition, we investigate the influence of external flow on the dynamics by varying flow parameters, like the flow exponent α and flow strength W_α. Our analysis highlights two anomalous power-law regimes, viz., subdiffusive (intermediate-time polymer stretching and flow-induced diffusion) and superdiffusive (long-time flow-induced diffusion). The anomalous long-time dynamics is governed by the temporal exponent ν of ASD, viz., $\nu = 2 - \alpha/2$. Compared to a linear polymer, the comb-of-comb network shows a shorter crossover time (from the subdiffusive to superdiffusive regime) but a reduced magnitude of ASD. Our theory displays an anomalous VACF in the random layered flows that scales as $t^{-\alpha/2}$. We show that the network with greater total mass moves faster.

DOI: 10.1103/PhysRevE.94.062503

I. INTRODUCTION

Chain topology and external flow fields are two important factors that have a profound impact on the dynamics of a single polymer in a solution. Significant theoretical advances have been made focusing on these two areas separately, i.e., investigating the influence of molecular architecture [1–10] and that of random flows [11–14] and random flows with mean shear [15,16] on the dynamics of a dilute polymer solution. Earlier studies on the absence of external flows focused mainly on the topological aspect where the role of the polymer structure is analyzed by varying the functionality or the generations and the length of the branches or spacers for various complex architectures, such as star polymers [1–4]; dendrimers [1–3,5,6,17]; dendrimers built from stars [7,18]; various kinds of fractal polymer networks, viz., the Sierpinski gasket [19,20] and Vicsek fractals (regular hyperbranched polymers) [8,9]; and random structures such as small-world networks (SWN) [10,21]. In contrast, the other simplified theoretical approach concerning the polymer dynamics in hydrodynamic flow mainly focuses on the flow characteristics using the elastic dumbbell model of a polymer [12–16] that does not take into account the architecture constraints, which limits its applicability to only linear chains. So there is a need to account for these important issues in one place, i.e., the role of hydrodynamic flow and chain architecture in the dynamics.

Understanding the dynamical properties of an isolated polymer in external flow fields has remained an outstanding problem owing to its wide range of biological applications, such as gene mapping [22,23], DNA separation [24,25], and the development and optimization of biological microfluidic devices [26]. Many significant experimental contributions have been achieved in understanding the flow-driven polymer dynamics [27–32]. Starting with the pioneering studies of Chu and collaborators for nonrandom elongational flow of a single chain [27,28], further investigations were performed for shear [29,30,33] and mixed flows [34]. Due to the difficulty to create a random flow in a microscopic-size volume, there was relatively little experimental progress until Groisman and Steinberg came up with the concept of elastic turbulence [35,36]. The polymer dynamics and statistics in a random flow with a shear component were studied experimentally [37] and numerically [15,16]. Experimental validation of the coil-stretch transition that is observed in the single polymer in random flows (as first predicted by Lumley [11]) was done by Gerashchenko *et al.* [38], and other works show aperiodic tumbling and stretching in the shear-preferred direction [37].

The fact that the branching significantly influences the conformational and dynamical properties of a single polymer in a solution [39–41] leaves exciting room to explore the dynamics of a polymer with complex underlying topologies. A way to do this is done using the generalized Gaussian structure (GGS) approach [42,43], which is an extension of the renowned Rouse model [44]. Based on this approach, different static and dynamic quantities of various flexible polymeric networks were studied [1–3,7–10,18–21,39]. Notable advances have been attained in understanding the link between the arbitrary topologies and their dynamical properties under the influence of external forces [1–10,17–21]. Remarkably, the influence of a step force on the stretching dynamics of the star and dendrimer with [2] and without hydrodynamic interaction (HI) [3] has been studied. The results suggest that at very short and long times, the displacement of the bead pulled by an external force has a constant velocity, while at intermediate times the influence of the underlying topology of the polymer on its dynamics is observed. Chen and Cai [6,17] determined the relaxation times and the normal modes of trifunctional dendrimers using the analytical method for the diagonalization of the connectivity matrix, while Biswas *et al.* [1,3] and Kant *et al.* [2] employed a numerical diagonalization procedure that showed excellent agreement with that obtained analytically. Another important class of polymeric structures is that of deterministic fractals modeled through finite Sierpinski-type networks. These fractal networks obey the scaling behavior

*rkant@chemistry.du.ac.in; http://people.du.ac.in/~rkant/

of the mechanical and dielectric relaxation patterns in the intermediate frequency range for a Rouse-type model (without HI) [19], while no scaling was seen for a Zimm-type model (with HI) [20]. Moreover, the dynamics of these types of fractals was shown to exhibit dependence on the spectral dimension [19,20]. In contrast to dendrimers and Sierpinski-type lattices, scaling does hold for Vicsek fractals both in the presence and the absence of HI [8,9]. While in the above-mentioned works the dynamics of the branched polymer was investigated in the presence of an electric field, there have been very few attempts to understand their structural and rheological properties under the hydrodynamic shear flow for stars [40,45] and dendrimers [41,46].

In the present work, we study the dynamics of a comb-of-comb network in the presence of random layered flows. Here we use the formalism developed in our previous paper [47] for arbitrary topology in external random flow. The comb resulting from the second generation ($g = 2$) of the hierarchy of the comb-of-comb network has extensively been synthesized, and its rheological properties have been studied [48–50]. The iterative comb-of-comb network is topologically constructed as follows: at each new step each bead of the entire network gets attached to the linear chain of the same length (for details refer to Sec. III). Based on our recent work where we developed the formalism for the dynamics of GGS under the influence of random layered flow fields [47], we follow here the particular case of the comb-of-comb network in order to understand and compare its dynamics with that of the linear chain and other important polymer networks like dendrimers. Our initial results have shown the sail boat behavior of polymers with the unexpected behavior of a polymer with a greater total mass (or size) moving faster than those with less mass (or size) in the random flow [47]. In the present work, we discuss the velocity autocorrelation function (VACF) and the average squared displacement (ASD) of the center of mass (c.m.) of a single comb-of-comb network in random flow. We use here the Matheron–De Marsily (MdM) model [51] for the random flow, which can mimic various flow conditions depending upon its flow statistics. Using this model, Oshanin and Blumen [52,53] investigated the dynamics of a Rouse (linear) polymer and showed that the ASD of the c.m. of the chain exhibits anomalous time dependence. The exponent which characterizes the growth of the ASD is dependent on the statistical properties of random flow. In a recent paper [54] the dynamics of comb-of-comb networks was studied by investigating properties like monomer displacement under constant force and mechanical relaxation moduli using Laplacian spectra. Another recent study was done using fluorescence microscopy on surface tethered DNA-comb under shear flow [55].

This paper is structured as follows: In Sec. II, we recall the mathematical formalism of the GGS model taking into account the statistical properties of the MdM flow pattern in order to understand the dynamical behavior of branched polymers under external random flow. We compute the generalized analytical expressions for the VACF and the ASD of the c.m. of branched polymers under external flow. Section III focuses on the discussion of our results and analyzing how these quantities depend on the underlying topologies of the comb-of-comb network and the random flow parameters. Moreover, we show the influence of the HIs on its dynamics. Finally, we summarize our paper with the conclusions in Sec. IV.

II. MATHEMATICAL APPROACH

In this section, we review the mathematical formalism for the dynamics of GGS in random layered flow reported in Ref. [54]. A GGS is viewed as consisting of N spherical beads connected t each other through harmonic springs; this is an extension of the classical Rouse approach [56]. The configuration of a GGS is denoted by the set of position vectors $\{R_i\}$, where $R_i(t) \equiv (R_{xi}(t), R_{yi}(t), R_{zi}(t)) \equiv (X_i(t), Y_i(t), Z_i(t))$ is the position vector of the ith bead at time t. Neglecting the HIs and excluding the volume effects, the dynamics of the ith bead of a GGS subjected to the external random force F_i is given by the linearized Langevin equation [56]:

$$\zeta \frac{\partial R_i(t)}{\partial t} + K \sum_{j=1}^{N} A_{ij} R_j(t) = f_i(t) + \delta_{\alpha Y} F_i, \tag{1}$$

where ζ is the friction coefficient of a single bead; $K = 3k_BT/b^2$ is the spring constant, with T being the temperature, k_B being the Boltzmann constant, and b being the mean distance between the beads; and $\mathbf{A} = \{A_{i,j}\}$ is the connectivity matrix of the GGS indicating beads that are directly connected to each other. The diagonal elements of $\mathbf{A}$, i.e., A_{mm} equals the number of bonds emanating from the mth bead, and its off-diagonal elements A_{mn} are -1 if m and n are connected and 0 otherwise. In Eq. (1), $f_i(t)$ is the random force on the ith bead. These random thermal forces arise as a result of collisions due to the ceaseless and irregular motion of beads in the surrounding solvent particles and are centered Gaussian processes with mean

$$\langle f(t) \rangle = 0, \tag{2}$$

and their correlation function follows the fluctuation-dissipation theorem:

$$\langle f_{i\alpha}(t) f_{j\beta}(t') \rangle = 2k_BT\zeta\, \delta_{ij}\, \delta_{\alpha\beta}\, \delta(t - t'). \tag{3}$$

In Eq. (1) F_i defines the force induced by the external random flow on the ith bead. To account for random flow we use the MdM model as shown in Fig. 1 (also see Refs. [52,53]). This type of model can be represented as a series of different layers parallel to each other and perpendicular to any axis, say, here the X axis. While the orientation of the force vector is fixed within each layer, it varies randomly when going from one layer to the other. In general the force or the velocity vector (as $V = F/\zeta$) is parallel to the Y axis, and the X and Z components of the velocity vector are equal to zero. The Y component is taken to be the random function of the X coordinate:

$$V_Y(X, Y, Z) = V[X]. \tag{4}$$

The random function $V[X]$ is assumed to be a Gaussian random function with the mean

$$\overline{V[X]} = 0 \tag{5}$$

and covariance

$$\overline{V[X_1]V[X_2]} = V_0^2\, \phi(|X_1 - X_2|). \tag{6}$$

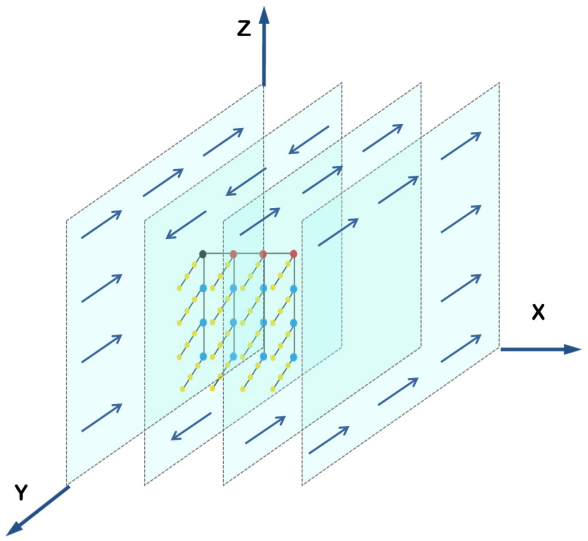

FIG. 1. Schematic diagram of a comb-of-comb network in the Matheron–De Marsily (MdM) flow pattern. The orientation of the velocity vector is a random function of the X variable and is constant within each layer.

The overline represents the average over the random flow configurations, V_0 is the rms velocity of the flow, and the correlation function ϕ defines the correlation between various layers of the random flow. The random flow is assumed to be a stationary process; hence, it depends only on the separation between the two layers. Another important transform of quantity ϕ is the power spectrum $\mathcal{Q}(K)$, which is defined by the Fourier integral,

$$\phi(|X_1 - X_2|) = \int_{-\infty}^{\infty} dK\, \mathcal{Q}(K) \exp[iK(X_1 - X_2)]. \quad (7)$$

We can model different types of flow behaviors by choosing a specific form of the power spectrum $\mathcal{Q}(K)$. The dimension of $\mathcal{Q}(K)$ is length. The important case for a random layered flow field is that of a power-law power spectrum,

$$\mathcal{Q}(K) = \frac{l_f}{2\pi} |l_f K|^{\alpha-1} = \frac{W_\alpha |K^{\alpha-1}|}{2\pi\, V_0^2} \qquad (0 < \alpha \leqslant 1), \quad (8)$$

where l_f is defined as the persistence length of the flow. It is a measure of the distance between two layers of flow. Here α signifies the type of flow or the persistence of the random flow. Its value lies between 0 and 1. $\alpha = 1$ indicates the δ correlated flow. As the value of α decreases, the long-range correlation effects are enhanced; in other words, it shows higher persistence of the flow. The prefactor W_α of the power-law power spectrum is a composite quantity which can be defined as

$$W_\alpha = V_0^2 l_f^\alpha. \quad (9)$$

Therefore, the power-law power spectrum of random flow can mimic different types of flows which are generated with a change in α, V_0, and l_f. The correlation function for the power-law spectrum in Eq. (8) can be obtained as

$$\phi(|X_1 - X_2|) = \frac{\Gamma(\alpha)\cos(\alpha\pi/2)}{\pi\, V_0^2} \frac{W_\alpha}{|X_1 - X_2|^\alpha}, \quad (10)$$

where $\Gamma(\alpha)$ is the gamma function. Equation (10) has a long-range algebraic distance-dependent correlation [53]. However, the simplest example of the power spectrum is a constant value, which is the white noise power spectrum, defined as

$$\mathcal{Q}(K) = \frac{l_f}{2\pi}. \quad (11)$$

When $\alpha \to 1$, Eq. (8) reduces to Eq. (11). This spectrum corresponds to the original MdM model with a δ correlated flow field,

$$\phi(|X_1 - X_2|) = l_f\, \delta(X_1 - X_2), \quad (12)$$

where δ is the Dirac delta function.

Usually, the strength of flow in a polymeric system is characterized by the Weissenberg number (Wi), which is the measure of the relative intensity of elastic relaxation and stretching and is defined as the product of the longest relaxation time τ_P of the polymer and the characteristic velocity gradient V_0/l_f:

$$\mathrm{Wi} = \frac{V_0}{l_f}\tau_P. \quad (13)$$

To observe the influence of the polymeric structure on random flow, l_f must be much greater than the Kuhn segment length and can be of the order of the radius of gyration R_g of the polymeric structure. Since τ_P depends on the branching structure of the polymer, Wi will depend on the structure of a polymer of a given molecular weight.

The convenient and general way to find the solution of Eq. (1) is to write a matrix representation for different components of R_i, viz., X_i, Y_i, Z_i. At this stage it is important to emphasize that the simplicity of this problem arises due to the decoupling of the components of R_i. Let us remark here that in Eq. (1), the Kronecker delta function $\delta_{\alpha Y}$ is used with external convective force F_i, which vanishes in the X and Z directions, where the bead undergoes only conventional diffusive motion, while it takes a value of 1 in the Y direction, where it experiences the external convective force superposed on the diffusive motion. Therefore, we will be interested in studying the dynamics on only the Y axis. Now, the matrix representation of Eq. (1) for the Yth component of the position vector is given by

$$\frac{\partial \mathbf{Y}(t)}{\partial t} + \sigma \mathbf{A}\mathbf{Y}(t) = \frac{1}{\zeta}[\mathbf{f}(t) + \mathbf{F}(t)], \quad (14)$$

with $\sigma = K/\zeta$, $\mathbf{R} \equiv (R_1, R_2, \ldots, R_N)^T$, $\mathbf{f} \equiv (f_1, f_2, \ldots, f_N)^T$, and $\mathbf{F} \equiv (F_1, F_2, \ldots, F_N)^T$, where T denotes the transposed vector. The solution of Eq. (14) represents the bead motion due to both the external flow and the thermal fluctuation:

$$\mathbf{Y}(t) = \frac{1}{\zeta}\int_{-\infty}^{t} dt' \exp[-\sigma(t - t')\mathbf{A}][\mathbf{f}(t') + \mathbf{F}(t')]. \quad (15)$$

Now the expression for the ASD of the c.m. of a branched polymer $\overline{\langle Y_{\mathrm{c.m.}}^2(t)\rangle}$, where the angular brackets represent

averaging over the thermal forces f_i and the overline represents the averaging over various configurations of random flow F_i [the expression for the displacement of the c.m. and the complete steps are explicitly reported in Ref. [54]], is

$$\overline{\langle Y^2_{c.m.}\rangle} = \frac{2k_BT}{N\zeta}t + \frac{V_0^2}{N^2}\int_0^t dt' \int_0^t dt'' \sum_{m,n}\int_{-\infty}^{\infty} dK\,\mathcal{Q}(K) \times \langle e^{iK[X_m(t')-X_n(t'')]}\rangle. \tag{16}$$

We can define the quantity called the dynamic structure factor $g(K,t',t'')$ as

$$g(K,t',t'') = \frac{1}{N}\sum_{m,n}\langle e^{iK[X_m(t')-X_n(t'')]}\rangle. \tag{17}$$

For a Gaussian process with $t' = 0$, Eq. (17) is simplified using cumulant expansion [56], where we have used the fact that $\langle X_i(t')\rangle = 0$ for all i:

$$g(K,0,t'') = \frac{1}{N}\sum_{m,n} e^{-K^2\langle[X_m(0)-X_n(t'')]^2\rangle/2}. \tag{18}$$

Now, since the random process $X_m(t') - X_n(t'')$ is stationary in time, it holds that

$$X_m(t') - X_n(t'') = X_m(0) - X_n(|t'-t''|). \tag{19}$$

Moreover, due to the symmetry of the dynamic structure factor with respect to the time variables, the ASD of the center of mass can be written as

$$\overline{\langle Y^2_{c.m.}\rangle} = \frac{2k_BT}{N\zeta}\,t + \frac{2\,V_0^2}{N}\int_0^t dt' \int_0^{t'} dt'' \int_{-\infty}^{\infty} dK\,\mathcal{Q}(K)\,g(K,t''). \tag{20}$$

The first term in Eq. (20) indicates the diffusion of the N-bead polymeric system due to the thermal fluctuations, and it does not possess any structural information, while the second term depends upon the structure of the polymer through the dynamic structure function. The additional contribution to the ASD arises due to the weighted average from the power spectrum and dynamic structure function.

Let us remark here that the function

$$E(t'') = \frac{1}{N}\int_{-\infty}^{\infty} dK\,\mathcal{Q}(K)\,g(K,t'') \tag{21}$$

is the VACF. Now substituting $\mathcal{Q}(K)$ from Eq. (8) and the dynamic structure factor $g(K,t'')$ using Eq. (18) into Eq. (21) and performing the integral, the formal expression for the VACF for long-range correlated random flows is obtained as

$$E(t'') = \frac{2^{\frac{\alpha}{2}-1}\,W_\alpha\,\Gamma(\alpha/2)}{\pi\,V_0^2\,N^2}\sum_{m,n}[X_m(0) - X_n(t'')]^2\rangle^{-\alpha/2}, \tag{22}$$

where $W_\alpha = V_0^2\,l_f^\alpha$ and has dimensions of (length)$^{2+\alpha}$/(time)^2. For the white noise spectrum ($\alpha = 1$), the expression simplifies as

$$E(t'') = \frac{W_\alpha}{V_0^2\,N^2}\sum_{m,n}\{2\pi\,\langle[X_m(0) - X_n(t'')]^2\rangle\}^{-1/2}. \tag{23}$$

Now in order to find the explicit expression of VACF $E(t'')$, one needs to find the difference correlation function $\langle[X_m(0) - X_n(t'')]^2\rangle$, calculated as

$$\langle[X_m(t') - X_n(t'')]^2\rangle = \langle[X_m(t')]^2\rangle + \langle[X_n(t'')]^2\rangle - 2\langle[X_m(t')X_n(t'')]\rangle. \tag{24}$$

In general the time correlation function for the X component is given by

$$\begin{aligned}\langle \mathbf{X}(t')\mathbf{X}^T(t'')\rangle &= \frac{1}{\zeta^2}\int_{-\infty}^{t'} dt_1 \int_{-\infty}^{t''} dt_2 e^{-\sigma(t'-t_1)\mathbf{A}}\langle f(t_1)f^T(t_2)\rangle e^{-\sigma(t''-t_2)\mathbf{A}} \\ &= \frac{2k_BT}{\zeta}\int_{-\infty}^{t''} dt_2 e^{-\sigma(t'+t''-2t_2)\mathbf{A}}.\end{aligned} \tag{25}$$

In writing Eq. (25) we have used the fact that $f(\mathbf{A})^T = f(\mathbf{A})$. We now diagonalize $\mathbf{A}$ in the usual fashion by determining first N linearly independent normalized eigenvectors $\mathbf{Q_i}$ of $\mathbf{A}$, so that $\mathbf{AQ}_i = \lambda_i\mathbf{Q}_i$. We set $\mathbf{Q} \equiv (\mathbf{Q}_1,\mathbf{Q}_2,\ldots,\mathbf{Q}_N)$ and have $\mathbf{AQ} = \mathbf{Q\Lambda}$, where $\mathbf{\Lambda}$ is the diagonal matrix whose elements are λ_i. Then,

$$\mathbf{A} = \mathbf{Q\Lambda Q^{-1}} \tag{26}$$

holds, with $\mathbf{Q^{-1}}$ being the inverse of $\mathbf{Q}$. From Eq. (26) any function of $\mathbf{A}$ can be written as

$$f(\mathbf{A}) = \mathbf{Q}f(\mathbf{\Lambda})\mathbf{Q^{-1}}. \tag{27}$$

Especially, one has

$$\exp(\mathbf{A}t) = \mathbf{Q}\exp(\mathbf{\Lambda}t)\mathbf{Q^{-1}}. \tag{28}$$

Thus, Eq. (25) can be written in terms of these eigenvalues and eigenvectors as

$$\langle \mathbf{X}(t')\mathbf{X}^T(t'')\rangle = \frac{2k_BT}{\zeta}\int_{-\infty}^{t''} dt_2 \mathbf{Q}\,e^{-\sigma(t'+t''-2t_2)\mathbf{\Lambda}}\mathbf{Q^{-1}}. \tag{29}$$

We use the operator $\mathbf{u}_m \equiv (0,0,\ldots,1,\ldots,0,0)$ to project out the mth element in Eq. (29) to write the expression of Eq. (24) as

$$\begin{aligned}&\langle[X_m(t') - X_n(t'')]^2\rangle \\ &= \mathbf{u}_m\langle \mathbf{X}(t')\mathbf{X}^T(t')\rangle\mathbf{u}_m^T + \mathbf{u}_n\langle \mathbf{X}(t'')\mathbf{X}^T(t'')\rangle\mathbf{u}_n^T \\ &\quad - 2\mathbf{u}_m\langle \mathbf{X}(t')\mathbf{X}^T(t'')\rangle\mathbf{u}_n^T \\ &= \frac{2k_BT}{\zeta}\sum_i\Bigg[\int_{-\infty}^{t'} dt_2\,Q_{mi}e^{-2\sigma(t'-t_2)\lambda_i}\,Q^{-1}_{im} \\ &\quad + \int_{-\infty}^{t''} dt_2\,Q_{ni}\,e^{-2\sigma(t''-t_2)\lambda_i}\,Q^{-1}_{in} \\ &\quad - 2\int_{-\infty}^{t''} dt_2\,Q_{mi}e^{-\sigma(t'+t''-2t_2)\lambda_i}\,Q^{-1}_{in}\Bigg].\end{aligned} \tag{30}$$

Isolating the $\lambda_1 = 0$ term in Eq. (30) and integrating it while taking into account that $Q_{m1} = Q^{-1}_{1m} = 1/\sqrt{N}$ for all values of m, we obtain

$$\begin{aligned}&\langle[X_m(t') - X_n(t'')]^2\rangle \\ &= \frac{2k_BT}{N\zeta}|t'-t''| + \frac{k_BT}{\sigma\zeta}\sum_{i\neq 1}\big[Q_{mi}\,Q^{-1}_{im}/\lambda_i \\ &\quad + Q_{ni}\,Q^{-1}_{in}/\lambda_i - 2\,Q_{mi}e^{-\sigma|t'-t''|\lambda_i}\,Q^{-1}_{in}/\lambda_i\big].\end{aligned} \tag{31}$$

In order to obtain the ASD of the c.m. of GGS, $E(t'')$ has to be integrated with respect to the time variables while taking into account the coefficient and the thermal fluctuation term [see Eqs. (20)–(22)]. Since the difference correlation function in Eq. (31) has a complicated form, the time integral of $E(t'')$ cannot be solved exactly. For that one needs to expand the integrand for short- and long-time limits. For the short-time limit, i.e., at times much less than the Rouse relaxation time τ_R ($t'' \ll \tau_R$), the expansion will dominantly have information about individual segment or bead relaxation as it shows ballistic motion of individual beads. Also, the velocity vector stays more or less constant at short times, so it takes a time much larger than τ_R in order to encounter various layers along the X axis. Since, in this short-time regime, the dynamics does not possess any structural information about the polymer, we focus only on the long-time limit that gives all the information about the topology of the polymer and its interaction with the random flow.

For the long-time limit, i.e., $|t' - t''| > \tau_R$, Eq. (31) can be simplified by dropping the exponential term and substituting $t' = 0$ as

$$\langle [X_m(0) - X_n(t'')]^2 \rangle \approx \frac{2k_BT}{N\zeta} t'' + \frac{k_BT}{\sigma\zeta} \times \sum_{i\neq 1} \left[Q_{mi} Q^{-1}_{im}/\lambda_i + Q_{ni} Q^{-1}_{in}/\lambda_i \right]. \tag{32}$$

Substituting Eq. (32) into Eq. (22), we get the final expression for the VACF for the long-time limit:

$$E(t'') = \frac{W_\alpha\, \Gamma(\alpha/2)}{2\pi\, V_0^2\, N^2 (D_R)^{\alpha/2}\, (t'')^{\alpha/2}} \times \sum_{m,n} \left(1 + \frac{\pi^2\, \tau_R}{2Nt''} \sum_{i\neq 1} C_i^{mn} \right)^{-\alpha/2}. \tag{33}$$

In Eq. (33), the Rouse relaxation time is defined as $\tau_R = \zeta b^2 N^2/3\pi^2 k_B T$. The diffusion coefficient is defined as $D_R = k_B T/N\zeta$, and $C_i^{mn} = Q_{mi} Q^{-1}_{im}/\lambda_i + Q_{ni} Q^{-1}_{in} \lambda_i$. Now performing time integrals of $E(t'')$ in Eq. (33) and using Eqs. (20) and (21), we get the final explicit expression for the ASD of the c.m. of GGS for the long-time limit:

$$\overline{\langle Y^2_{c.m.} \rangle} = \frac{2k_BT}{N\zeta}\, t + \frac{4W_\alpha\, \Gamma(\alpha/2)}{\pi(4-\alpha)(2-\alpha)} \left(\frac{\zeta N}{k_BT} \right)^{\alpha/2} t^{2-\alpha/2} \times \left\{ 1 - \mathcal{C}_1 \left(\frac{\pi^2 \tau_R}{2t} \right)^{1-\alpha/2} + \mathcal{C}_2 \left(\frac{\pi^2 \tau_R}{2t} \right) - \cdots \right\}, \tag{34}$$

where $\mathcal{C}_1$ and $\mathcal{C}_2$ are polymer-structure- and flow-type-dependent coefficients. $\mathcal{C}_2$ is the coefficient of stretching, while $\mathcal{C}_1$ is the coefficient of counterstretching induced by the random flows, and they are defined as

$$\mathcal{C}_1 = \frac{4-\alpha}{2} \left(\frac{1}{N} \right)^{3-\alpha/2} \sum_{m,n} \left(\sum_{i\neq 1} C_i^{mn} \right)^{1-\alpha/2},$$

$$\mathcal{C}_2 = \frac{4-\alpha}{2N^3} \sum_{m,n} \left(\sum_{i\neq 1} C_i^{mn} \right).$$

The first term in Eq. (34) signifies the drift due to the thermal fluctuations, and the second term represents polymer dynamics in the external random flows. Since in the long-time limit, the contribution due to the thermal fluctuations is negligibly small, the first term can be neglected. The anomalous drift and stretching in the polymer dynamics are enacted through the second term. This term has three components: (i) the stretch induced by random flow, (ii) the dynamic contravening of stretch due to random flow, and (iii) the drift motion of the stretched polymer. Equating the first and second components, we obtain a characteristic maximum stretching time t_s, after which the curtailment of polymer stretching occurs, and t_s is defined as

$$t_s = \left(\frac{\mathcal{C}_2}{\mathcal{C}_1} \right)^{2/\alpha} \left(\frac{\pi^2 \tau_R}{2} \right). \tag{35}$$

For time less than t_s, subdiffusive behavior is observed due to the flow-induced internal dynamics of the polymer. Equating the stretch and the drift components, we obtain another characteristic time t_d of anomalous drift motion, which is defined as

$$t_d = \mathcal{C}_2 \left(\frac{\pi^2 \tau_R}{2} \right). \tag{36}$$

The polymer follows superdiffusive behavior above the drift crossover time t_d.

Substituting $\alpha = 1$ in Eq. (34), we directly calculate the ASD for the δ correlated flow:

$$\overline{\langle Y^2_{c.m.} \rangle} = \frac{2k_BT}{N\zeta} t + \frac{4W_\alpha}{3} \left(\frac{\zeta N}{\pi k_BT} \right)^{1/2} t^{3/2} \times \left\{ 1 - \mathcal{C}_1 \left(\frac{\pi^2 \tau_R}{2t} \right)^{1/2} + \mathcal{C}_2 \left(\frac{\pi^2 \tau_R}{2t} \right) - \cdots \right\}, \tag{37}$$

where

$$\mathcal{C}_1 = \frac{3}{2} \left(\frac{1}{N} \right)^{5/2} \sum_{m,n} \left(\sum_{i\neq 1} C_i^{mn} \right)^{1/2},$$

$$\mathcal{C}_2 = \frac{3}{2N^3} \sum_{m,n} \left(\sum_{i\neq 1} C_i^{mn} \right).$$

Therefore, in the long-time limit, Eqs. (34) and (37) give the final results for the ASD of the center of mass of the GGS in the case of flows with long-range correlation and δ correlation, respectively.

III. DYNAMICS OF THE COMB-OF-COMB NETWORK

We introduce another class of macromolecules with treelike structure built in an iterative way, referred to as the comb-of-comb network $C_{g,r}$, obtained after the gth generation, with each branch consisting of r beads, as shown in Fig. 2. Starting with $g = 0$, it consists of a single bead. For generation $g = 1$, $C_{1,r}$ is a linear chain with r beads; consecutively, for $g = 2$ it refers to that of a comb structure with both a linear backbone and side arms consisting of r beads each. Topologically speaking, the network $C_{g,r}$ begins with a single bead which gets attached to a chain consisting of $r - 1$ beads. At each

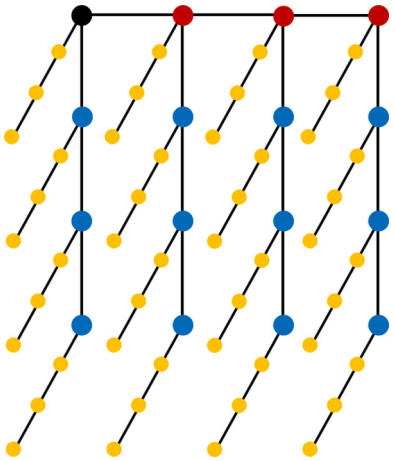

FIG. 2. Schematic diagram of the comb-of-comb network $C_{g,r}$ with $r = 4$ and $g = 3$.

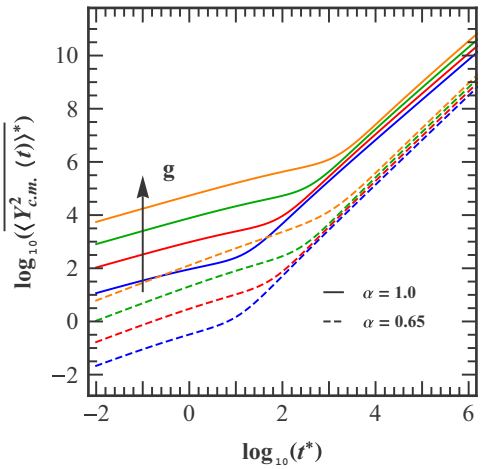

FIG. 3. Dynamics of the center of mass of the comb-of-comb network $C_{g,r}$ under the influence of external random flow, plotted in double logarithmic scales $\overline{\langle Y^2_{c.m.}\rangle}^* = \overline{\langle Y^2_{c.m.}\rangle}/\langle R^2_g\rangle$ vs $t^* = \sigma t$ for the networks $C_{g,r}$ for varying generations g, i.e., $g = 2,3,4$, and 5 (from below) and fixed $r = 3$. We indicate the cases where $\alpha = 1$ (delta correlated flow) by solid lines and where $\alpha = 0.65$ (moderately correlated) by dashed lines for $W_\alpha = 5 \times 10^{-11}$ a.u.

new generation each bead of the entire network gets attached to the chain of $r - 1$ beads. In general, $C_{g,r}$ is obtained by attaching a new chain with $r - 1$ beads to each of the beads of the $C_{g-1,r}$ network. So the total number of beads in $C_{g,r}$ is $N = r^g$. Figure 2 shows schematically the comb-of-comb network with $g = 3$ and $r = 4$. Compared to another class of treelike macromolecules, the dendrimer, which is only densely packed at the periphery, the comb-of-comb network is a dense structure as a whole.

In this section we study the dynamics of the center of mass of the comb-of-comb network by using the expressions for the VACF [Eq. (33)] and the ASD [Eqs. (34) and (37)] obtained in the previous section. In order to determine the VACF and the ASD, both the eigenvalues λ_i and the eigenvectors Q_i of adjacency matrix $\mathbf{A}$ are required, which we obtained by numerically diagonalizing the matrix $\mathbf{A}$. We used *Mathematica* software for the numerical calculations and for generating the graphs. In this section we will discuss the influence of varying topology and the random flow parameters in understanding the dynamics of the comb-of-comb network.

To generate our graphs, we have assumed that each bead and spring are made up of N_0 Kuhn segments so that the effective friction coefficient $\zeta = N_0\,\zeta_0$, and the effective segment length (made up of N_0 segments) becomes $b = \sqrt{N_0}\,b_0$, where ζ_0 is the friction coefficient of each Kuhn segment and b_0 is the Kuhn segment length. Taking $N_0 \simeq 100$, the longest relaxation time turns out to be of the order of 10 s, which is a typical experimental time scale for large realistic polymers [35,36]. The other parameters that we have used are $\zeta_0 = 0.35 \times 10^{-6}$ dyn s/cm, $b_0 = 6.7 \times 10^{-8}$ cm, and $k_BT = 4.11 \times 10^{-14}$ ergs at 298 K. The ASD in all figures is scaled with respect to the square of the radius of gyration of the linear chain, $\langle R^2_g\rangle = Nb^2/6$.

In Fig. 3 we display the effect of topology of the $C_{g,r}$ network on its dynamics by varying its generations g, i.e., $g = 2,3,4$, and 5 with fixed $r = 3$. Using Eq. (34), the ASD of the center of mass $\overline{\langle Y^2_{c.m.}\rangle}^*$ is plotted against the time t^*, where in both cases the asterisk indicates that the quantities are given in dimensionless units, so that $\overline{\langle Y^2_{c.m.}\rangle}^* = \overline{\langle Y^2_{c.m.}\rangle}/\langle R^2_g\rangle$ and $t^* = \sigma t$. Here the scaling of the ASD is done with $\langle R^2_g\rangle$ of the linear chain with total beads $N = 9$. As we can see from Fig. 3, it highlights two anomalous power-law regimes: intermediate- and long-time regimes. The intermediate-time regime corresponds to the internal motion of the chain where $\overline{\langle Y^2_{c.m.}\rangle} \propto t^\nu$, where $\nu < 1$; that is, it shows subdiffusive behavior. It is observed that the magnitude of the ASD increases with generation g of the $C_{g,r}$ network with constant r. Physically, this is evident because with increasing g, the total mass of $C_{g,r}$ grows, and as a result, there is greater stretching because now there are more bonds that undergo stretching, which results in an increase in the ASD of the center of mass. The maximum stretching of $C_{g,r}$ with $g = 5$ is about four times that of the network with $g = 2$. Now, with the influence of the external random flow the time dependence of the ASD is enhanced in the long-time regime, where it exhibits superdiffusive behavior with $\nu > 1$, attributed to the overall diffusion of the polymer. Again, in this time regime, the magnitude of the ASD is greater for $C_{g,r}$ with greater g; that is, $C_{g,r}$ with greater total mass moves faster than that with lower total mass, a result that is in agreement with the results of Refs. [52,53] for the Rouse chain and for stars and dendrimers [47]. Another important observation is the delay in the drift crossover time t_d, from the subdiffusive to superdiffusive regime, with an increase in generation g. This can be understood because with increasing g, the total mass increases, and therefore, the internal dynamics last longer for the longer time, hence delaying crossover to the overall diffusive regime.

The other aspect that we understand from Fig. 3 is the impact of the external random flow on the dynamics of the comb-of-comb network. For this we study the same system, i.e., the $C_{g,r}$ network with varying $g = 2,3,4$, and 5 and fixed $r = 3$, for different values of flow exponent α. We indicate the cases with $\alpha = 1$ (δ correlated flow) by solid lines and with $\alpha = 0.65$ (moderately correlated) by dashed lines for

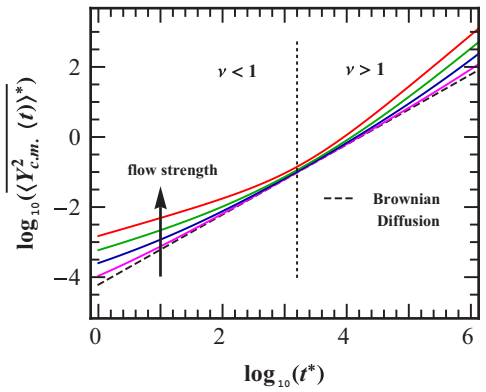

FIG. 4. Influence of varying flow strength depicted in two anomalous time regimes, plotted in logarithmic scales $\overline{\langle Y^2_{c.m.}\rangle}^*$ vs t^* for the comb-of-comb network with $g = 4$; $r = 4$ for $\alpha = 1$ and varying W_α, i.e., $W_\alpha = (0,1,4,11,30) \times 10^{-18}$ a.u. (from bottom to top).

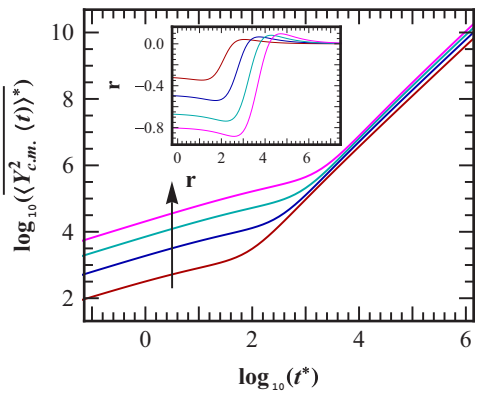

FIG. 5. Dynamics of the center of mass of the $C_{g,r}$ network under the influence of external random flow. The main figure gives the double logarithmic plot of dimensionless ASD $\overline{\langle Y^2_{c.m.}\rangle}^*$ vs dimensionless time t^* for fixed generation $g = 3$ and varying r, i.e., $r = 3,4,5$, and 6 (from bottom to top). Here the ASD is scaled with R_g corresponding to the linear polymer with total beads $N = 27$. The flow parameters are $\alpha = 1$ and $W_\alpha = 5 \times 10^{-11}$ a.u. The inset displays the dynamical topological ratio of average squared displacement r as a function of t^* for the network with the same color code.

$W_\alpha = 5 \times 10^{-11}$ arbitrary units (a.u.). We observe that as we go from δ correlated towards strongly correlated flow, there is a decrease in the magnitude of the ASD, while the temporal dependence of the ASD increases as there is an increase in the slope in both time regimes which is also evident from Eq. (34). The best power fits $\overline{\langle Y^2_{c.m.}\rangle} \propto t^\nu$ for $\alpha = 1$ give $\nu = 0.46 \pm 0.01$ in the intermediate-time regime and $\nu = 1.54 \pm 0.01$ in the long-time regime, and for $\alpha = 0.65$ it gives $\nu = 0.62 \pm 0.01$ in the intermediate-time regime and $\nu = 1.69 \pm 0.01$ in the long-time regime.

Another significant flow parameter that has a great impact on the dynamics of the flexible comb-of-comb network is the flow strength W_α. Figure 4 presents the influence of varying flow strength by plotting the scaled ASD vs scaled time for increasing values of W_α, i.e., $W_\alpha = (0,1,4,11,30) \times 10^{-18}$ a.u. It is observed that increasing the strength of the external random flow exhibits an increase in the anomalous behavior in both the time regimes, i.e., an increase in the subdiffusive and superdiffusive behaviors in the intermediate- and long-time regimes, respectively. This is evident from the slope of the curve ν, which decreases in the intermediate-time regime and increases in the long-time regime with an increase in W_α. Interestingly, under the limit of negligible flow strength ($W \to 0$), the ASD reduces to the conventional diffusive motion, viz., Brownian diffusion (see black dashed line in Fig. 4); that is, it becomes linearly dependent on time. So it is worthwhile to mention that the presence of the external flow results in the change of the conventional diffusive behavior to subdiffusive in the intermediate-time regime and superdiffusive in the long-time regime.

Along similar lines, the topology effects of the $C_{g,r}$ network on its dynamics by varying r, i.e., $r = 3,4,5$, and 6 with fixed $g = 3$, are presented in Fig. 5. As expected, the magnitude of ASD increases with r as total mass increases in both the time regimes. Again, we observe the shift in t_d with the increase in total molecular weight of the $C_{g,r}$ network. The intermediate-time regime clearly shows the influence of varying topology of the $C_{g,r}$ network in the presence of external random flow. Another important and useful measure that displays the relative difference in the dynamics of the $C_{g,r}$ network compared to that of the linear polymer is the dynamical topological ratio $r(t)$. It gives the ratio of the ASD of the c.m. of the $C_{g,r}$ network to that of a linear polymer with the same total number of beads N:

$$r = \frac{\overline{\langle Y^2_{c.m.}\rangle}_{C_{g,r}}}{\overline{\langle Y^2_{c.m.}\rangle}_{\text{Linear}}}. \tag{38}$$

In the inset of Fig. 5 we have plotted in double logarithmic scales $r(t)$ as a function of t^* for the $C_{g,r}$ network with the same color code as in the main plot. As the total mass of $C_{g,r}$ increases, the time at which the minimum and the maximum of $r(t)$ are observed is shifted to the right. Moreover, the values of the minimum and maximum peaks get enhanced with the total mass of the network.

Next, in Fig. 6, we display the long-time dependence of the ASD of the c.m. of the $C_{g,r}$ network of various r and g with fixed total beads $N = 256$ under the influence of external random flow. Here again scaled ASD (with $\langle R_g^2\rangle$ of a linear chain with 256 beads) is plotted against dimensionless time t^* in double logarithmic scales using Eq. (37). As we can see from Fig. 6, the influence of the underlying topology is unraveled in the intermediate-time regime, where the magnitude of the ASD of the $C_{g,r}$ network is observed to be smaller than the linear analog ($r = 256, g = 1$), while as N is fixed, the long-time regime becomes completely independent of the topology, resulting in the merging of all the curves together. Moreover, compared to a linear polymer, the comb-of-comb network shows the drift crossover time shifted towards the left; that is, in the case of the $C_{g,r}$ network the crossover time to reach the superdiffusive regime arrives earlier than in the linear polymer case. This can be understood as the comb-of-comb network being more compact than the linear analog with the same total mass, and the overall diffusive

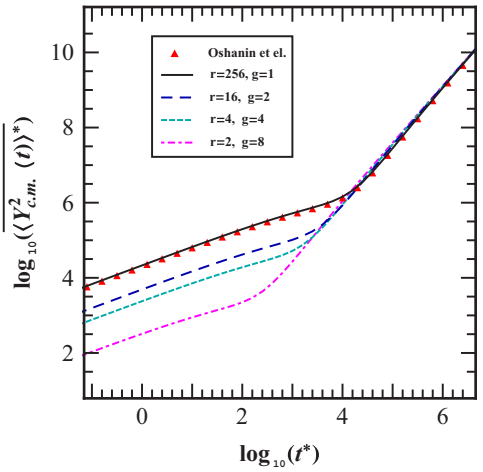

FIG. 6. Average squared displacement of the c.m. of the comb-of-comb network $C_{g,r}$ of various r and g under the influence of external MdM flow and a comparison with Oshanin and Blumen's [53] continuum model result for a linear chain (shown by red triangles). Plotted is $\overline{\langle Y^2_{c.m.}\rangle}^*$ vs dimensionless time t^* in double logarithmic scales for $\alpha = 1$. All networks have the same total number of beads, $N = 256$.

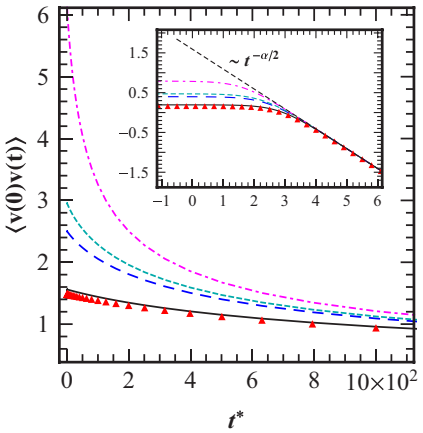

FIG. 7. Influence of topology on VACF for various $C_{g,r}$ networks with fixed total beads $N = 64$ and flow exponent $\alpha = 1$ and a comparison with Oshanin and Blumen's [53] continuum model result for a linear chain (shown by red triangles). Plotted is $\langle v(0)v(t)\rangle$ vs dimensionless time t^* using Eq. (33) for various network topologies: $g = 6$, $r = 2$ (dot-dashed magenta curve); $g = 3$, $r = 4$ (short-dashed cyan curve); $g = 2$, $r = 8$ (long-dashed blue curve); and $g = 1$, $r = 64$ (solid black curve). Here the $g = 1$, $r = 64$ network corresponds to the linear polymer. The inset shows $\langle v(0)v(t)\rangle$ as a function of t^* in double logarithmic scales. Here the black dotted line indicates the $t^{-\alpha/2}$ decay.

motion of the comb-of-comb network becomes easier and therefore arrives earlier. To validate our theoretical formalism for a limiting case of a linear polymer, we have compared our discrete model results with the Oshanin and Blumen [53] continuum model results for the Rouse chain. In Fig. 6, the red triangles refer to the continuum model results [refer to Eq. (59) of Ref. [53]], and the black solid line indicates our result given by Eq. (37). As shown, our discrete model excellently captures the results of the continuum model for a linear chain.

Figure 7 shows the decay of the VACF for various comb-of-comb networks $C_{g,r}$ with a constant value of total beads $N = 64$ and flow exponent $\alpha = 1$. Plotted is $\langle v(0)v(t)\rangle$ vs dimensionless time t^* using Eq. (33) for various networks: $r = 2$, $g = 6$ (dash-dotted magenta curve); $r = 4$, $g = 3$ (short-dashed cyan curve); $r = 8$, $g = 2$ (long-dashed blue curve); and $r = 64$, $g = 1$ (solid black curve). Here the $r = 64$, $g = 1$ network corresponds to the linear polymer. As we see from Fig. 7, it shows the rapid decay of VACF at intermediate time along with the long-time algebraic tail. The asymptotic long-time behavior is of the form $t^{-\alpha/2}$ [see Eq. (33)]. Also we observe that decreasing the compactness of the network results in faster decay of the VACF curve in the intermediate-time regime. Thus, the linear polymer being the least compact leads to the fastest decay of the VACF curve. Moreover, we have compared the VACF results of our discrete model [Eq. (33)] shown by the black solid line in Fig. 6 with the Oshanin and Blumen continuum model results [refer to Eq. (58) of Ref. [53]] for a Rouse chain indicated by the red triangles. Again, as observed, our results are shown to be in excellent agreement with continuum model results for a linear chain. The inset shows the same plot of $\langle v(0)v(t)\rangle$ vs t^* in double logarithmic scales, where the black dashed line corresponds to the $t^{-\alpha/2}$ decay. With an increase in the compactness of the network, the maximum value of the VACF increases in early time. So compared to the comb-of-comb network, the linear polymer exhibits a lower magnitude of the VACF with faster decay of the curve in the intermediate-time regime.

Besides the effect of topology, the VACF is also influenced by the hydrodynamic flow that is shown in Fig. 8 for the $C_{g,r}$ network with $g = 3$ and $r = 4$. Using Eq. (33), we have plotted $\langle v(0)v(t)\rangle$ vs dimensionless time t^* for various values of flow exponent α, i.e., $\alpha = 0.4$, 0.5, and 0.6 (from top to bottom). In general, the VACF curve decays with the long-time algebraic tail that scales as $t^{-\alpha/2}$. Quantitatively, an increase in α results in faster decay of the VACF curve, as observed in Fig. 8.

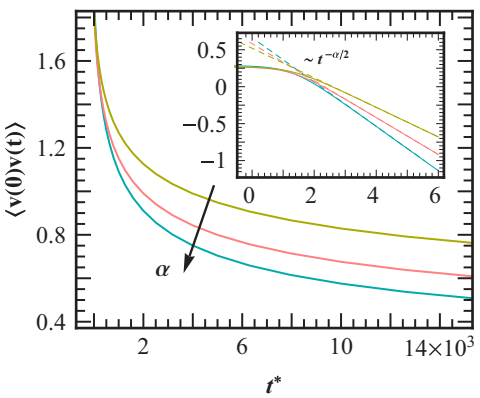

FIG. 8. Influence of external flow on VACF of the $C_{g,r}$ network with $g = 3$ and $r = 4$. Plotted is $\langle v(0)v(t)\rangle$ vs dimensionless time t^* using Eq. (33) for various values of flow exponent α, i.e., 0.4,0.5,0.6 (from top to bottom). The inset shows $\langle v(0)v(t)\rangle$ as a function of t^* in double logarithmic scales for various α with the same color code as in the main plot. Here the dashed lines indicate the $t^{-\alpha/2}$ decay for corresponding α values.

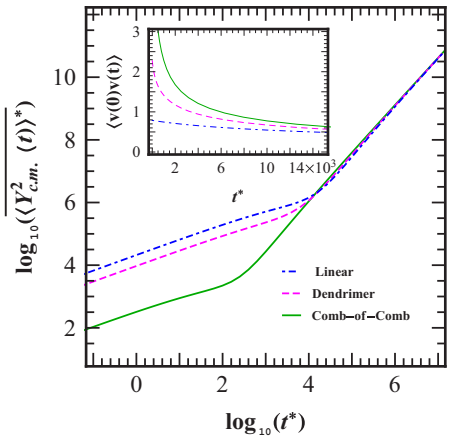

FIG. 9. Comparison of the dynamics of the comb-of-comb network and those of a dendrimer and a linear polymer with almost the same total number of beads in external random flow. The main plot shows $\overline{\langle Y^2_{c.m.}\rangle}^*$ vs t^* in double logarithmic scales for $C_{8,2}$ (solid green curve), $C_{1,256}$ corresponding to the linear polymer (dot-dashed blue curve), and a dendrimer with spacer $p = 12$, generation $G = 3$ (dashed magenta curve). The inset depicts the VACF vs time for topologies with same line and color code.

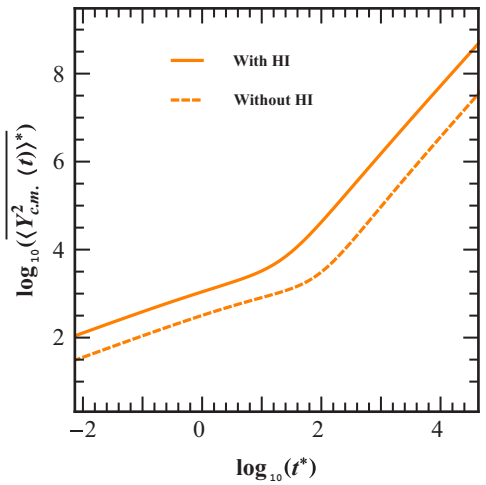

FIG. 10. Comparison of the dynamics of the comb-of-comb polymer with HI (solid line) and without HI (dashed line) with $r = 3$ and $g = 3$. Plot of $\overline{\langle Y^2_{c.m.}\rangle}^*$ (scaled $\overline{\langle Y^2_{c.m.}\rangle}$ with $\langle R^2_g\rangle$ of the linear polymer with the same total number of beads $N = 27$) vs t^* in double logarithmic scales with $\alpha = 1$ and $W_\alpha = 5 \times 10^{-11}$ cm^3/s^2.

This can be understood as the higher value of α signifying antipersistence behavior of the flow; that is, the random nature of the flow is changing rapidly. The long-range correlation effects are observed with an increase in the persistence flow behavior, i.e., smaller α, therefore resulting in the slowing down of the decay. The double logarithmic plot of the VACF is shown in the inset in Fig. 8. Here the dashed lines indicate the $t^{-\alpha/2}$ decay for the corresponding α values. Another flow parameter is the flow strength W_α that occurs in Eq. (33) as the multiplicative factor; therefore, it alters only the magnitude of the VACF curve and does not change the decay time.

Finally, we compare the dynamics of the comb-of-comb network with that of a dendrimer and a linear polymer with almost same total number of beads ($N = 256$ for the comb-of-comb network and linear polymer and $N = 253$ for the dendrimer) under the external MdM flow with $\alpha = 1$ and $W_\alpha = 5 \times 10^{-11}$ cm^3/s^2 (see Fig. 9). The main plot of Fig. 9 displays in double logarithmic scales $\overline{\langle Y^2_{c.m.}\rangle}^*$ vs t^* for the comb-of-comb network with $r = 2$ and $g = 8$ (solid green curve), the dendrimer with spacer $p = 12$ and generation $g = 3$ (dashed magenta curve), and the linear polymer (dot-dashed blue curve). In this plot we observe that the influence of the topology of the polymer is unraveled in the intermediate-time regime, where the magnitude of the ASD follows the trend with the linear polymer showing the maximum value, followed by the dendrimer, and the comb-of-comb showing the minimum value of the ASD. Since all three topologies considered have almost the same total mass, all the curves merge at long times, showing no dependence on topology at long times. Although the magnitude of the ASD of the $C_{g,r}$ network is the lowest among the three topologies, t_d for $C_{g,r}$ occurs faster than for the dendrimer and linear polymer. This is because the overall size of the $C_{g,r}$ network is the minimum; in other words, it is the most compact of the three topologies with the same total mass. As a result, the overall diffusion becomes easier in the case of the comb-of-comb network, and therefore, t_d arrives earlier. The inset in Fig. 9 depicts the VACF vs time for topologies with same line and color code. As observed, the VACF curve decays fastest for the linear polymer (dot-dashed blue line), followed by the dendrimer (dashed magenta line), while the slowest decay is observed for the comb-of-comb network (solid green line).

Contribution of HIs

The results presented in the previous sections investigated the dynamics of the comb-of-comb network in the absence of HIs. So the purpose of introducing this section is to give a brief idea of what the impact of the incorporation of HIs is on the dynamics of the comb-of-comb network in the external random flow. A detailed mathematical formalism and description are beyond the scope of the present paper and will be presented in a separate publication. Now as we are aware of the fact that the dynamical behavior of a polymer in a dilute solution is strongly affected by the nonlinear and long-range hydrodynamic interactions, it is pertinent to include this effect and quantify its relevance. Various analytical theories have been developed that reveal the influence of hydrodynamic interactions on the various conformational and dynamical properties of polymers in a solution [56–58]. Zimm extended the Rouse theory in order to take into account the HI effects using the preaveraged approximation [56,58]. He obtained the theory of the relaxation behavior of long polymer chains in the absence of excluded volume effects. Later, the Zimm theory was extended to study in detail the intrinsic viscosity and the relaxation modes of branched polymers such as stars and dendrimers [59].

We employ a similar methodology to obtain our results with the inclusion of HIs using a preaveraged approximation. Figure 10 depicts the influence of including HIs on the ASD dynamics of the comb-of-comb network in double logarithmic scales with $r = 3$ and $g = 3$. Here the Zimm case (with HIs)

and the Rouse case (without HIs) are shown as solid and dashed lines, respectively. The results reveal that while no qualitative change is observed, there is only a quantitative change in the dynamics of the comb-of-comb network with the inclusion of HIs in the external random flow. There are some key points of observation. First, taking HIs into account results in an increase in the magnitude of the ASD that is supposed to arise because there is an additional contribution of HIs that results in the faster displacement of the polymer. A further examination reveals that the inclusion of the HIs speeds up the stretch dynamics, and thus, the overall drift occurs faster, which is shown by the crossover time, which is shorter for the Zimm case than the Rouse case. This can be understood by the fact that the longest relaxation times given by the smallest nonvanishing eigenvalues are shorter in the Zimm case than in the Rouse case.

IV. CONCLUSIONS

In summary, our results show the influence of random flow on the dynamics of a single comb-of-comb network with varying topologies. The modeling of flexible branched polymers is done within the framework of the GGS approach, while the random flow is accounted for through the MdM model. Here we have numerically analyzed the dynamics through quantities like the ASD and VACF. On the basis of our analysis, there appear to be distinct commonalities and differences between the comb-of-comb network of varying topologies and its linear analog in random flows. Both linear and comb-of-comb networks show two anomalous power-law behaviors in the intermediate- and long-time regimes of the ASD. The dynamics in the intermediate-time regime is observed due to the flow-induced stretching, counterstretching, and drift of the polymer structure. The collective effect of these processes causes subdiffusive behavior. The dynamics in the long-time regime is due to the random-flow-induced drift of the stretched polymer and follows superdiffusive behavior. These dynamic behaviors have two characteristic times: maximum stretching crossover time t_s and anomalous drift crossover time t_d.

The drift crossover time (from the subdiffusive to superdiffusive regime) arrives earlier in the case of the comb-of-comb network than in the linear polymer with the same total mass. The magnitude of ASD increases for topologies generated with an increase in generation g of the comb-of-comb network. The nature of intermediate-time subdiffusive and long-time superdiffusive behaviors is preserved, while their crossover times increase with an increase in g. In our analysis, we showed that the comb-of-comb network with greater total mass moves faster in a random layered flow. This conclusion is similar to the one obtained for a linear Rouse chain in Refs. [52,53] and stars and dendrimers in Ref. [47]. On the other hand, this observation is in contrast to the case of nonrandom flows where the smaller polymers move faster than larger polymers [53]. The influence of topologies, with the same total mass, is unraveled in the intermediate-time regime. The temporal exponent ν of ASD that is indicative of the degree of the anomaly is shown to be dependent on only the flow parameters, i.e., α and W_α, while it is independent of the mass and the topology of polymer. With an increase in the value of α, the magnitude of the ASD increases, while the temporal exponent of the ASD decreases in both time regimes. With an increase in W_α, the temporal exponent decreases in the intermediate-time regime (more subdiffusive) and increases in the long-time regime (more superdiffusive). Moreover, our theory predicts anomalous VACF in the random layered flows with the long-time algebraic tail that scales as $t^{-\alpha/2}$. Increasing α or the antipersistence behavior of flow results in faster decay of the VACF curve. The intramolecular hydrodynamic interactions move the onset of the topological effects to earlier times; that is, the overall diffusive behavior occurs more quickly in the presence of HIs with the enhanced magnitude of the ASD. We hope that the analytical results presented here will be helpful in experiments to understand the dynamics of branched polymers under external flows and will stimulate efforts with such systems in numerically simulated random flows [60].

ACKNOWLEDGMENTS

D.K. acknowledges Council of Scientific and Industrial Research, India for providing the JRF and SRF scholarship and the University of Delhi for providing a University Teaching Assistantship (UTA). R.K. is grateful to the University of Delhi for an R & D grant and a Science and Engineering Research Board, India grant.

[1] P. Biswas, R. Kant, and A. Blumen, J. Chem. Phys. **114**, 2430 (2001).
[2] R. Kant, P. Biswas, and A. Blumen, Macromol. Theory Simul. **9**, 608 (2000).
[3] P. Biswas, R. Kant, and A. Blumen, Macromol. Theory Simul. **9**, 56 (2000).
[4] J. Roovers and B. Comanita, Adv. Polym. Sci. **142**, 179 (1999).
[5] F. Ganazzoli, R. LaFerla, and G. Raffaini, Macromolecules **34**, 4222 (2001).
[6] C. Cai and Z. Y. Chen, Macromolecules **30**, 5104 (1997).
[7] C. Satmarel, C. von Ferber, and A. Blumen, J. Chem. Phys. **124**, 174905 (2006).
[8] A. Blumen, C. von Ferber, A. Jurjiu, and T. Koslowski, Macromolecules **37**, 638 (2004).
[9] A. Jurjiu, T. Koslowski, C. von Ferber, and A. Blumen, Chem. Phys. **294**, 187 (2003).
[10] A. A. Gurtovenko and A. Blumen, J. Chem. Phys. **115**, 4924 (2001).
[11] J. L. Lumley, Symp. Math. **9**, 315 (1972).
[12] E. Balkovsky, A. Fouxon, and V. Lebedev, Phys. Rev. Lett. **84**, 4765 (2000).
[13] M. Chertkov, Phys. Rev. Lett. **84**, 4761 (2000).
[14] M. Martins Afonso and D. Vincenzi, J. Fluid Mech. **540**, 99 (2005).
[15] K. Turitsyn, J. Exp. Theor. Phys. **105**, 655 (2007).

[16] M. Chertkov, I. Kolokolov, V. Lebedev, and K. Turitsyn, J. Fluid Mech. **531**, 251 (2005).
[17] Z. Y. Chen and C. Cai, Macromolecules **32**, 5423 (1999).
[18] C. Satmarel, C. von Ferber, and A. Blumen, J. Chem. Phys. **123**, 034907 (2005).
[19] A. Blumen and A. Jurjiu, J. Chem. Phys. **116**, 2636 (2002).
[20] A. Jurjiu, Th. Koslowski, and A. Blumen, J. Chem. Phys. **118**, 2398 (2003).
[21] A. Blumen, A. A. Gurtovenko, and S. Jespersen, J. Non-Cryst. Solids **305**, 71 (2002).
[22] E. Y. Chan *et al.*, Genome Res. **14**, 1137 (2004).
[23] D. C. Schwartz, X. Li, L. I. Hernandez, S. P. Ramnarain, E. J. Huff, and Y. K. Wang, Science **262**, 110 (1993).
[24] P. S. Doyle, J. Bibette, A. Bancaud, and J. L. Viovy, Science **295**, 2237 (2002).
[25] J. Han and H. G. Craighead, Science **288**, 1026 (2000).
[26] M. D. Graham, Annu. Rev. Fluid Mech. **43**, 273 (2011).
[27] T. T. Perkins, D. E. Smith, and S. Chu, Science **276**, 2016 (1997).
[28] D. E. Smith and S. Chu, Science **281**, 1335 (1998).
[29] D. E. Smith, H. P. Babcock, and S. Chu, Science **283**, 1724 (1999).
[30] P. LeDuc, C. Haber, G. Boa, and D. Wirtz, Nature (London) **399**, 564 (1999).
[31] C. M. Schroeder, H. P. Babcock, E. S. G. Shaqfeh, and S. Chu, Science **301**, 1515 (2003).
[32] S. R. Quake, H. Babcock, and S. Chu, Nature (London) **388**, 151 (1997).
[33] S. Gerashchenko and V. Steinberg, Phys. Rev. Lett. **96**, 038304 (2006).
[34] H. P. Babcock, R. E. Teixeira, J. S. Hur, E. S. G. Shaqfeh, and S. Chu, Macromolecules **36**, 4544 (2003).
[35] A. Groisman and V. Steinberg, Phy. Rev. Lett. **86**, 934 (2001).
[36] A. Groisman and V. Steinberg, Nature (London) **405**, 53 (2000).
[37] Y. Liu and V. Steinberg, Europhys. Lett. **90**, 44005 (2010).
[38] S. Gerashchenko, C. Chevallard, and V. Steinberg, Europhys. Lett. **71**, 221 (2005).
[39] A. A. Gurtovenko and A. Blumen, Adv. Polym. Sci. **182**, 171 (2005).
[40] M. Ripoll, R. G. Winkler, and G. Gompper, Phys. Rev. Lett. **96**, 188302 (2006).
[41] S. V. Lyulin, A. A Darinskii, A. V. Lyulin, and M. A. J. Michels, Macromolecules **37**, 4676 (2004).
[42] H. Schiessel, Phys. Rev. E **57**, 5775 (1998).
[43] H. Schiessel, Chr. Friedrich, and A. Blumen, *Applications of Fractional Calculus in Physics*, edited by R. Hilfer (World Scientific, Singapore, 1999).
[44] P. E. Rouse, J. Chem. Phys. **21**, 1272 (1953).
[45] S. P. Singh, A. Chatterji, G. Gompper, and R. G. Winkler, Macromolecules **46**, 8026 (2013).
[46] A. Nikoubashman and C. N. Likos, Macromolecules **43**, 1610 (2010).
[47] D. Katyal and R. Kant, Phys. Rev. E **91**, 042602 (2015).
[48] M. Kapnistos, D. Vlassopoulos, J. Roovers, and L. G. Leal, Macromolecules **38**, 7852 (2005).
[49] D. R. Daniels, T. C. B. McLeish, B. J. Crosby, R. N. Young, and C. M. Fernyhough, Macromolecules **34**, 7025 (2001).
[50] M. Kempf, D. Ahirwal, M. Cziep, and M. Wilhelm, Macromolecules **46**, 4978 (2013).
[51] G. Matheron and G. De Marsily, Water Resour. Res. **16**, 901 (1980).
[52] G. Oshanin and A. Blumen, Phys. Rev. E. **49**, 4185 (1994).
[53] G. Oshanin and A. Blumen, Macromol. Theory Simul. **4**, 87 (1995).
[54] H. Liu, Y. Lin, M. Dolgushev, and Z. Zhang, Phys. Rev. E **93**, 032502 (2016).
[55] D. J. Mai, A. B. Marciel, C. E. Sing, and C. M. Schroeder, ACS Macro Lett. **4**, 446 (2015).
[56] M. Doi and S. F. Edwards, *The Theory of Polymer Dynamics* (Clarendon, Oxford, 1986).
[57] J. G. Kirkwood and J. Riseman, J. Chem. Phys. **16**, 565 (1948).
[58] B. H. Zimm, J. Chem. Phys. **24**, 269 (1956).
[59] B. H. Zimm and R. W. Kilb, J. Polym. Sci., Part B **34**, 1367 (1996).
[60] A. Smirnov, S. Shi, and I. Celik, J. Fluids Eng. **123**, 359 (2001).